1st International Conference on Computer Vision (ICCV1987), London, UK, pp. 191-200, IEEE Computer Society Press, Washington, doi: 10.5281/zenodo.13126

Image Sequence Analysis of Complex Physical Objects: Nonlinear Small Scale Water Surface Waves

Bernd Jähne

Institute for Environmental Physics, University of Heidelberg
Im Neuenheimer Feld 366, D-6900 Heidelberg, West Germany

Abstract

Image sequence analysis is a promising tool to study the physics of waves propagating on water surfaces. Physical knowledge about water waves is used to develop two different approaches to sequence analysis: motion is determined (a) in the Fourier space and (b) by a new method based on a directio-pyramidal decomposition in the space domain. Both methods proof to be interesting tools for investigating the nonlinear nature of water surface waves. Image sequence analysis of such objects opens an exciting interdisciplinary research area between computer vision and the physics of nonlinear phenomena.

1. Introduction

Small scale water surface waves (wavelengths 2 mm to 2 m) receive more and more attention in environmental sciences. This is because they are involved in a number of current research topics. One of the most important is backscattering of microwaves, emitted from satellites, by the wavy ocean surface. The intensity of the backscattered microwaves is determined by small scale waves. Knowledge about the basic interrelations between these waves, wind speed, and the backscattered signal opens a wide field for remote sensing [12]. Another topic concerns the energy flux from atmosphere to ocean via waves, which is still known only crudely [16]. Finally, waves considerably enhance the transfer of gaseous pollutants between atmosphere and ocean [8].

Without going more into details it can be imagined easily that these questions are of importance for such relevant topics as global energy cycling (i.e. climate) and exchange of pollutants. Yet there are many open questions concerning the physics of water surface waves. This is not surprising. On the one hand, waves are a complex nonlinear and stochastic phenomenon. On the other hand, the measuring technique is not adequate. Up to now, most experimental work has been done with probes measuring the time series of wave height or wave slope at a single point [6]. It is beyond doubt that such a technique fails to determine all effects of the waves related to their two-dimensional spatial structure.

Image sequence analysis of waves is the appropriate instrument to study the water surface waves, since the amplitude $a = a(\mathbf{x},t)$ of waves is given as a function of two space coordinates and one time coordinate.

Processing of image sequences from water surface waves has been used as an experimental tool only by one research group until now. Gotwols, Keller and Irani processed image sequences of small gravity waves both in the field [4], and in wind/wave facilities [9]. But so far their analysis has been restricted to the calculation of two- and three-dimensional mean power spectra ($S(\mathbf{k})$ and $S(\mathbf{k},\omega)$). The phase velocity as a function of the wavenumber is the only additional parameter extracted from these data.

Therefore it remains a challenging task to analyse wave image sequences in more detail. Since these objects are quite different from natural scenes, many interesting new questions arise and new paths have to be gone. But in contrast to natural scenes, this way is well guided by the knowledge about the object "wave": the hydrodynamic laws.

This paper is an extension of an earlier one describing the potentialities of image sequence analysis for two topics in environmental physics more generally [7]. Here image sequence processing of water surface waves is discussed in detail and preliminary results are reported. The basic new properties of the wave scenes are pointed out and are contrasted with natural scenes. Based on this knowledge two approaches to image sequence analysis are represented. We will discuss possibilities and limits of image sequence analysis in the Fourier space and introduce a new approach based on a directio-pyramidal decomposition of the sequences.

2. Moving Object "Water Surface Waves"

Motion Observation in the Space Domain

Figures 1 and 2 show two examples of wave image sequences taken in the large wind/wave facility of the Institut de Méchanique Statistique de la Turbulence (IMST), Marseille. The waves are observed perpendicularly to the water surface and their slope

is shown as different grey or color levels using an appropriate illumination technique [6]. This set up ensures that the two dimensional wave propagation on the water surface is projected onto the image plane. Motion on the image plane directly reflects motion at the water surface and does not contain any ambiguity by projections as for a three dimensional scene.

Consequently, the whole class of projection problems for motion analysis is bypassed. But another basic difficulty appears. It can best be expressed by the simple question:

What are the objects we see moving?

Indeed, this is the key question which turns out to be very difficult and to contain much of the physics of the waves. It is illustrated with the image sequence shown in Figures 1 and 2.

Especially from Figure 2 it can be seen that the wave field consists of components with various wavelengths propagating with different velocities and in different directions. The observed slope pattern results from the interference of all these differently moving components. Therefore the greyvalues cannot be regarded as well defined individual object points as for a rigid object. The sequences in Figures 1 and 2 also show how fast the slope pattern changes with time especially in the small scales.

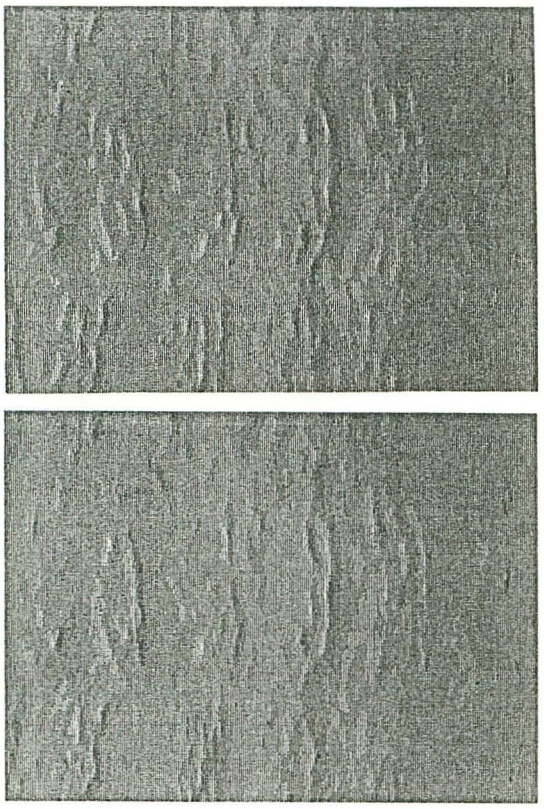

Figure 1: A wave image pair taken with a wave following visualization system moving with 25 cm/s in wind direction. The time interval between the two images is 40 ms, the sector shown is 15 cm times 20 cm, and the wind is blowing from the right to the left. The waves shown are initial waves obtained after turning on a wind speed of 6.5 m/s.

Consequently, the image sequences consist of "objects" changing their shape. The size of these objects is not well defined. The wave image sequences may be compared with the 3D-motion of several transparent objects in different distances from the camera with the restriction that their motion is parallel to the image plane. In 3D-motion objects change their shape by velocity components perpendicularly to the image plane. "Wave packets" change their shape by the physical laws governing them. The life time of individual "objects" is limited because of dynamic interaction processes.

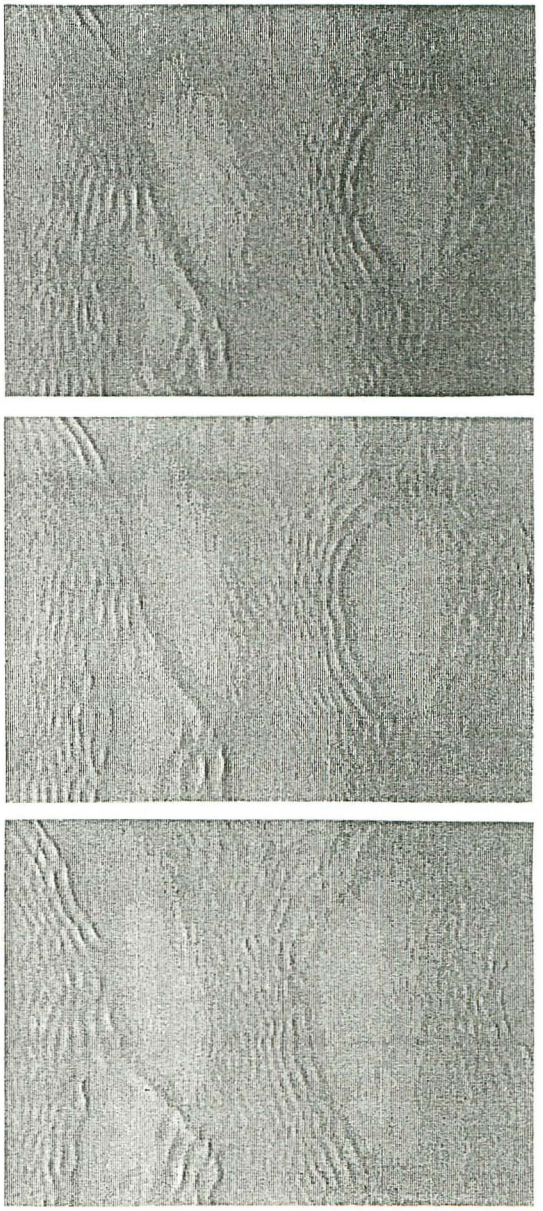

Figure 2: Same as Figure 1, but showing the waves several seconds later. The time difference between the first and second image is 40 ms, between the first and third image 160 ms. A comparison between the first and third image shows that the wave trains propagate with different velocities.

An interactive procedure between physical modeling and image sequence processing will be necessary in order to determine the actual spatial and temporal characteristics of the objects the motion of which we are observing. This will be the red thread to be followed in the rest of this section.

First we can conclude that it does not make much sense just to use the original greylevel picture for image sequence analysis. Let us illustrate which information a displacement vector field of the greylevel image would contain. Every algorithm determining a displacement vector field is most sensitive to the steepest changes in greylevels. So it mainly represents the motion of the small scales which is the sum of the phase velocity of small scale waves and the orbital velocities of larger waves modulating it. These two components in the motion cannot be separated since only one displacement vector field is obtained.

Therefore we have to ask for other representations of the wave images in which a more detailed sequence analysis can be carried out. This discussion is guided by the physics of the waves.

Motion observation in the Fourier Domain

We start our considerations from the basic fact that waves of different wavelengths λ respectively wavenumbers $\mathbf{k}$ ($k = 2\pi/\lambda$) move independently with different phase velocities. Then these components are the individual objects we are searching for. The space domain is not a good representation, since they are spread over large areas superposing each other. This directly implies that they are well distinguished and represented in the Fourier space. Here they are sharply located objects: one point represents the amplitude and phase of a plane wave with the wavenumber $\mathbf{k}$. In conclusion, a Fourier transformation separates our wave images into independent objects and the motion analysis can be carried out easily in the Fourier space. This situation is in clear contrast to natural scenes, where motion analysis in the Fourier space does not make sense, as soon as there are more than one individually moving object in the scene.

The Nonlinear Nature of Water Waves

If waves were a linear phenomenon, we would have solved the problem of image sequence analysis of water waves. But the real difficulties are introduced by the nonlinear nature of water waves. First, the nonlinearity causes a wide variation of interaction processes between waves of different wavenumbers $\mathbf{k}$ limiting spatial and temporal scales of the individual wavenumbers. Second, motion of different wavenumbers may be coupled, so that quasi-rigid but spatially limited objects may exist.

With respect to image sequence analysis it is instructive to summarize the most important interaction processes for a wind wave field on the ocean [16].

1. The turbulent wind field puts energy into the wave field at different wavelengths: new waves of small scales are generated, other components are amplified.
2. Nonlinearity implies that waves of different wavenumbers cannot superimpose each other without disturbance. This process is called (nonlinear) wave-wave interaction and causes energy exchange between waves of different wavelengths as well as the generation of a third wave with another wavenumber.
3. The stability of waves decreases with their steepness. To an increasing extent waves loose energy which is transferred to turbulent motions. Larger waves break visibly with bubble entrainment, but also smaller waves can decay into turbulence ("micro-scale wave breaking" [1]).

These three processes basically determine the energy circulation in the wave field and therefore are the key to the research topics discussed in the introduction. There is a *source* (energy input by wind), a *distribution mechanism* (nonlinear wave-wave interaction) and a *sink* (decay into turbulence). For given conditions the wave field develops to a stationary mean spectrum where all energy fluxes balance each other in the mean.

Image sequence analysis should not just yield some kind of displacement vector field. It should rather determine these interaction processes, i.e. answer questions as

1. How much energy is transferred from the wind field into the waves at which wavelength?
2. Between which scales are the dominant wave-wave interactions?
3. At which scales do waves mainly decay into turbulence?

Generally, it is the aim of the analysis of wave image sequences to reveal their nonlinear nature. In this relation the question of a suitable representation of the waves is of importance. This representation, in turn, directly reflects the physical nature of the objects. In the following sections two approaches are discussed.

3. Global Representation in Fourier Space

This representation can be used as long as the interactions can be regarded as only small a disturbance of a linear superimposition. Then, as already discussed, the individual "object" is still wide spread in time and space and remains a small "object" in Fourier space.

Determination of Displacement Vectors in Fourier Space

Motion of a plane wave in the space domain results in a phase shift of the corresponding spectral density. This phase shift $\Delta\varphi$ is given by the cross-spectrum from two consecutive images

$$\Delta\varphi(\mathbf{k}) = \arctan \frac{Qu(\mathbf{k})}{Co(\mathbf{k})} \tag{1}$$

where the co-spectrum Co and the quad-spectrum Qu are the real and the imaginary part of the cross-spectral density, respectively. The corresponding phase velocity c and displacement vector $\mathbf{u}$ in the space domain are

$$c(\mathbf{k}) = \frac{\Delta\varphi(\mathbf{k})}{k\Delta t}, \qquad \mathbf{u}(\mathbf{k}) = \frac{\Delta\varphi(\mathbf{k})\mathbf{k}}{k^2} \tag{2}$$

It is important to note that for each wavenumber k in the Fourier space a homogeneous displacement vector field is obtained for the corresponding plane wave covering the whole space domain.

Determination of the Interaction

The interaction process can globally be characterized by the life time τ of the component. Since newly generated waves of the same wavenumber are incoherent to previously existing ones, the wave field becomes more and more incoherent with increasing time difference Δt between two consecutive frames. Cross-spectral analysis also yields the coherency

$$Coh^2(\mathrm{k}) = \frac{\langle Co\rangle^2 + \langle Qu\rangle^2}{\langle Pow\rangle^2} \tag{3}$$

where $\langle\cdots\rangle$ denotes the average of the spectral densities over many images. In this way the coherency allows an estimate of the interaction.

If the interaction is weak (i.e. changes the wave pattern only in scales $\tau \gg T$ and $\bar{x} = \tau c \gg \lambda$), then the interaction process can be linearized, and the coherency decreases exponentially with the lifetime τ.

Unfortunately another mechanism not transferring energy also decreases coherency. The phase velocity of small scale waves is modulated by the orbital velocities of larger waves, even if no interaction takes place. This effect leads to a variance in the phase velocity ($\langle\Delta^2 c\rangle$). The coherency decrease is proportional to this variance [6]

$$Coh^2 \approx 1 - (k\Delta t)^2\langle\Delta^2 c\rangle \tag{4}$$

A general problem in the coherency analysis is the limited area of the images. An object moving with a velocity u can be observed at most a period $\Delta t = l/u$, where l ist the size of the image. Typical phase velocities of 50 cm/s and picture sizes of 50 cm result in an observation time of about only 1 s, which is much too low. This problem has been solved with the image aquisition system. The whole wave visualization system used in the IMST wind/wave facility is mounted on a carriage, which can follow the wave field with adjustable speed of up to 1 m/s.

Results

Figure 3 shows the results of an cross-correlation analysis of 8 image pairs, from which one example is shown in Figure 1. After a 2D-FFT the mean spectral densities were calculated in a $(\ln k, \varphi)$ polar coordinate system. We chose 31 angular intervals from $-\pi/2$ to $\pi/2$ ($\Delta\varphi = \pi/31 = 5.8^o$). The logarithmic k-interval $\Delta \ln k = \Delta k/k$ has the same value as the angular interval resulting in a 10% k-resolution. Details of the analysis are described by *Huber* [5].

The $(\ln k, \varphi)$-representation for spectral densities offers two advantages. First, a considerable data reduction is achieved: For 256^2 pictures the 129×256 (k_x, k_y) matrix is mapped onto a 45×31 $(\ln k, \varphi)$ matrix, which is a reduction factor of more than 20. Second, the dynamic range of the Fourier coefficients is much lower. This effect is caused by the fact that the size of the discrete intervals increases with k^2. Consequently, also the spectral densities are multiplied by k^2 and can be displayed in a linear scale. Multiplying spectral densities with k^2 is a useful alternative to the conventional logarithmic scale used to display Fourier spectra. Indeed, it is more natural, since the limiting 2D-wave slope spectrum goes with k^{-2} [16], leading to a flat spectrum in the $(\ln k, \varphi)$ representation.

The power spectrum (Figure 3a) shows two peaks: a wide one at $k = 11.2$ cm^{-1} ($\lambda = 0.56$ cm) in the capillary wave region and a second, much narrower at $k = 2.1$ cm^{-1} ($\lambda = 3$ cm) in the gravity region. These two dominant wavelengths can also be seen in the space domain (Figure 1). Moreover the 2D-power spectrum contains the exact shape of the angular distribution of the waves. This is the basic new information contained in the 2D-wavenumber spectrum in comparison to the frequency spectrum derived from wave gauges measuring the wave slope or amplitude at a single point.

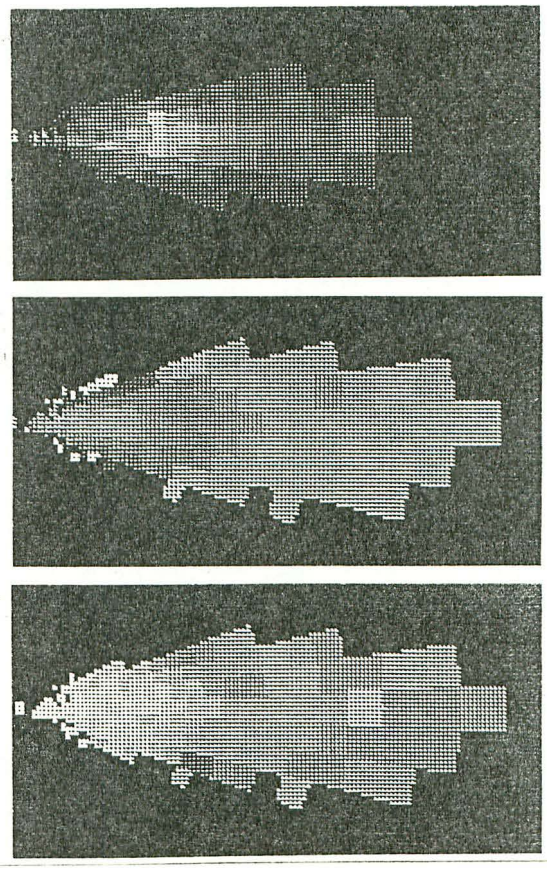

Figure 3: Mean power spectrum (a), phase velocity (b) and coherency (c) of image pairs from the wave patterns as in Figure 1. Only the right halfs of the symmetric spectra are shown. The ordinate is the along-wind wavenumber. All amplitudes are shown in linear scales with the following ranges: power spectrum: zero to maximum response, phase velocity: ± 3 cm/s (deviation from 25 cm/s, the velocity of the moving visualization system), coherency: 0 to 1.

Phase velocity and coherency are only shown in a window in which the spectral density is at least 1/32 of the peak density. The phase velocity (Figure 3b) can be measured quite sensitively. Since the image sequences are taken from a system moving with 25 cm/s, the whole velocity range in Figure 3b covers only the deviation from this value in a range of about ± 3 cm/s.

The coherency (Figure 3c) remains high up to the peak in the capillary range. Since the decrease in the coherency is caused by both the modulation and interaction processes, the life time of the individual wavenumbers cannot be calculated from just one image pair. It is rather necessary to calculate the coherency for different time differences Δt in order to separate both effects by their different time dependencies. Or, generally speaking, the image sequence analysis has to be extended to a true 3D-image, where time is the third coordinate.

Limits of Fourier Space Approach

Image sequence analysis in the Fourier space based on mean spectral densities has its limitations.

It is not possible to distinguish the different interaction processes by this analysis. The lifetime τ of one wavenumber is an integral information containing the interaction with all other wave numbers and the decay into turbulence. Nevertheless, a basic information is obtained. The lifetime and the mean energy density of a wave component yield the net energy flux density for this wavenumber.

Likewise all information about individual wave trains is lost by the averaging procedure. It can only be observed how long a certain wavenumber exists *in the mean*. This is not a sufficient analysis of the interaction processes if the nonlinearity becomes dominant. Then the Fourier space representation gives no useful picture of the wave field in the sense that a point in the Fourier space represents an object, i.e. a plane wave propagating — at least in first approximation — independently from other components of the wave field. Consequently, the whole approach discussed in this section breaks down under these circumstances.

From Figures 1 and 2 it is obvious that the interaction between small scale structures in the wave field is strong, since they rapidly change with time. Indeed, theoretical calculations show that wave-wave interactions are much stronger in the smaller scales (capillary-gravity range) than for large scales (pure gravity waves) [13].

4. Directio-Pyramidal Decomposition

Representation of Nonlinear Waves

In the case of stronger interaction we are confronted with the fact that the object is neither sharply located in the space domain nor in the Fourier domain. Then the scales in both domains to which a wave train extends become the characteristic parameter which is not known but which has to be determined. Moreover, we do not know, which scales move independently and which move coherently. If nonlinear interaction processes are dominant, then the phase relation between the components of different scales is of importance. But this is just the information lost by calculating mean spectral densities.

Therefore it is proposed first to separate the wave field into all components which *may* move independently, before the image sequence analysis is applied. Then in each level of the decomposition a displacement vector field can be calculated for instance with one of the established algorithms [14]. Afterwards coherent structures can be searched in space, within different pyramidal levels, and in time to extract the object scales, interactions between different scales, and the object life time.

A representation of the waves which separates wavenumbers but maintains as much spatial position as possible seems to be appropriate. These contradictionary demands (uncertainty principle) are optimally solved by the Laplace pyramid [2], [3]. It allows a separation of wavelengths in intervals of a factor 2 maintaining maximal possible spatial resolution. The factor 2 is especially useful to study nonlinear objects, because the first harmonic is located just one level lower in the pyramid.

But one problem remains with this decomposition. Figure 2 shows that wave components with similar scales but different directions are crossing each other. Such components are located in the same level of the pyramid though they are moving independently. Hence we propose an additional directional decomposition in each level of the pyramid to separate such components. A coarse directional decomposition is sufficient, since the waves normally cross each other nearly perpendicularly.

Filters for Directio-Pyramidal Decomposition

Directional filters have been proposed by many researchers (e.g. *Knutsson* [11], *Kunt et al.* [10]). Here we propose a simple set of directional filters simultaneously providing a pyramidal decomposition.

These filters are based on binomial kernels. The convolutions of the image with different kernels are combined which each other and result both in the directional components and the isotropic level of the pyramid.

The simplest construction scheme decomposes each level of the Laplace pyramid into two perpendicular directional components. Two 1D binomial smoothing filters, one along each axis, for instance

$$\mathcal{B}_x = \frac{1}{16}\left\{\begin{array}{ccccc} 1 & 4 & 6 & 4 & 1 \end{array}\right\}, \quad \mathcal{B}_y = \frac{1}{16}\left\{\begin{array}{c} 1 \\ 4 \\ 6 \\ 4 \\ 1 \end{array}\right\} \tag{5}$$

are convolved with each other to yield an isotropic smoothing kernel $\mathcal{B}$

$$\mathcal{B} = \mathcal{B}_x * \mathcal{B}_y \tag{6}$$

This isotropic kernel is used to calculate one level of the Laplace pyramid

$$\mathcal{L} = \mathcal{I} - \mathcal{B} \tag{7}$$

where I is the identity operator. The difference operator between the two 1D binomial kernels $\mathcal{B}_x$ and $\mathcal{B}_y$ is combined with the Laplace operator $\mathcal{L}$ to a new set of two directional kernels $\mathcal{D}_i$ adding up to $\mathcal{L}$.

$$\mathcal{D}_0 = \frac{1}{2}(\mathcal{L} + \mathcal{B}_x - \mathcal{B}_y), \quad \mathcal{D}_1 = \frac{1}{2}(\mathcal{L} - \mathcal{B}_x + \mathcal{B}_y) \tag{8}$$

with

$$\sum_{i=0}^{1} \mathcal{D}_i = \mathcal{L}$$

With additional binomial kernels along the diagonals

$$\mathcal{B}_{xy} = \frac{1}{4}\begin{Bmatrix} 0 & 0 & 1 \\ 0 & 2 & 0 \\ 1 & 0 & 0 \end{Bmatrix}, \quad \mathcal{B}_{-xy} = \frac{1}{4}\begin{Bmatrix} 1 & 0 & 0 \\ 0 & 2 & 0 \\ 0 & 0 & 1 \end{Bmatrix} \tag{9}$$

a separation in four directions is possible. The four binomial kernels ($\mathcal{B}_x$, $\mathcal{B}_y$, $\mathcal{B}_{xy}$, and $\mathcal{B}_{-xy}$) with equal variances (here $\sigma^2 = 1$) are combined to four identically constructed directional filters $\mathcal{B}_i$ with main axes in 22.5°, 67.5°, 102.5°, and 157.5° direction (steps of 45°)

$$\begin{aligned} \mathcal{B}_0 &= \mathcal{B}_x \mathcal{B}_{xy} \\ \mathcal{B}_1 &= \mathcal{B}_y \mathcal{B}_{xy} \\ \mathcal{B}_2 &= \mathcal{B}_y \mathcal{B}_{-xy} \\ \mathcal{B}_3 &= \mathcal{B}_x \mathcal{B}_{-xy} \end{aligned} \tag{10}$$

Consecutive filtering with two of these directional filters yields an isotropic binomial smoothing kernel with $\sigma^2 = 2$

$$\mathcal{B}' = \mathcal{B}_0 \star \mathcal{B}_2 = \mathcal{B}_1 \star \mathcal{B}_3 \tag{11}$$

This isotropical filter is used to calculate one level of the Laplace pyramid $\mathcal{L}' = I - \mathcal{B}'$. Finally the isotropic Laplace operator $\mathcal{L}'$ is combined with the set of directional filters $\mathcal{B}_i$ in (10) to a new set of directional filters $\mathcal{D}'_i$

$$\mathcal{D}'_i = \frac{1}{4}(\mathcal{L} + \mathcal{B}_i - \mathcal{B}_{i+2}) \quad \text{for} \quad 0 \le i < 4 \quad \text{with} \quad \sum_{i=0}^{3} \mathcal{D}'_i = \mathcal{L} \tag{12}$$

where $i + 2$ is calculated modulo 4.

It is also possible to construct a set of filters where the image is decomposed in directional components along the axes and diagonals (Figure 4)

$$\mathcal{D}''_i = \frac{1}{4}(\mathcal{L} + \mathcal{B}_i + \mathcal{B}_{i+1} - \mathcal{B}_{i+2} - \mathcal{B}_{i+3}) \quad \text{for} \quad 0 \le i < 4 \tag{13}$$

The frequency responses of these filters are shown in Figure 4. Despite the simple construction scheme a sufficient directional separation is obtained. The half width of all filters is 45°. The directional separation in only two components offers two basic advantages. First, all spatial frequencies perpendicular to the filter direction are completely removed. Second, the directional sensitivity is preserved up to the highest spatial frequencies.

This is not the case for the decomposition in four directions (Figure 4). At the highest spatial frequencies all filters give a uniform response. Nevertheless, this is no drawback of these directional filters since the highest frequencies are not existent in one level of the Laplace pyramid. Using an isotropic binomial filter with $\sigma^2 = 2$ for the construction of the Laplace pyramid results in maximal amplitude responses at a spatial frequency of 0.6 times the Nyquist frequency. At this frequency the directional separation is still sufficient.

A general benefit of these filters is the low cost. For one level of the Laplace pyramid including the directional decomposition in four directions with the kernels $\mathcal{D}'$ only 36 arithmetic operations (28 additions and 8 shift operations) are necessary per pixel if cascaded filtering with the elementary 1D binomial filter $\{11\}$ along the four directions is applied. This is a very low number of operations. A direct calculation of the directional components with the five 11×11 kernels ($\mathcal{D}'_i$ and $\mathcal{L}$) would need 1205 arithmetic operations (605 multiplications and 600 additions) per pixel.

RESULTS

Figures 5 and 6 show the decomposition of the wave images in Figure 1 and 2, respectively, in two directional components and three pyramidal layers as indicated in the figure caption.

Figure 5 does not only show the two dominant components, which have also been derived from the 2D-wavenumber spectrum. It also directly makes visible how the small capillary waves are modulated by the larger gravity wave including the phase relation of this interaction. In the cross-wind directional component, where the dominant along-wind component is filtered out, hidden crossing wave patterns are revealed, which are not visible in the original image (Figure 1). The crest of the gravity wave is disrupted along two horizontal lines. This is an example how 2D-instabilities of the waves can be investigated in detail with the proposed decomposition.

Crossing wave patterns in the cross-wind directional component can be observed even better in Figure 6. In addition, in some regions structures are preserved troughout the three levels of the Laplace pyramid. This indicates strong nonlinear interactions.

A decomposition in 4 directions with the filter set $\mathcal{D}'_i$ is shown in Figures 7 and 8. In these pictures the signum of the amplitude is displayed. In this representation characteristic structures can easily be traced through different directional components and the two levels of the Laplace pyramid. This allows direct conclusions how coherently or independently the different scales move.

The figures impressively demonstrate how much information can be obtained by directio-pyramidal decomposition. If now for each component a displacement vector field is calculated, it can easily be imagined that a powerful tool for the analysis of wave image sequences is at hand.

5. CONCLUSIONS

In this paper we introduced a new application for image sequence processing. The discussion shows that an interdisci-

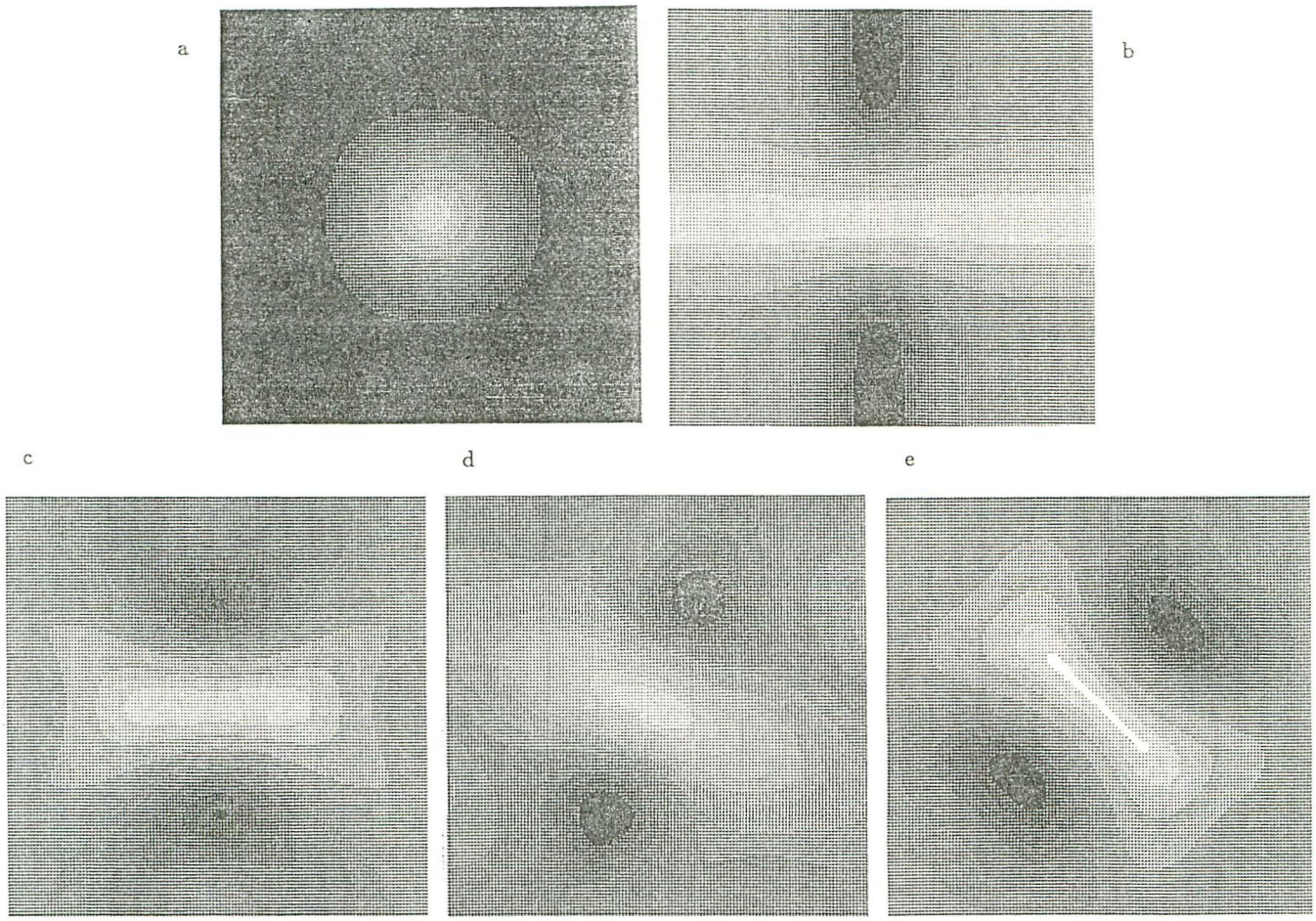

Figure 4: Frequency response of the filters used for directio-pyramidal decomposition. The shading is linear in 16 greylevels from zero to maximum response. a: Laplace kernel $\mathcal{L}$, b: $\mathcal{D}_1$, c: $\mathcal{D}_2''$ (90°), d: $\mathcal{D}_1'$ (67.5°), e: $\mathcal{D}_1''$ (45°).

plinary research area between experimental physics, environmental sciences, theoretical fluid dynamics, numerical mathematics, and computer vision is evolving. The two approaches presented here yield quite different results. On the one hand, the Fourier space approach allows a derivation of mean parameters of the image sequences, as mean spectral densities, phase velocities, and the coherency of the wave field. On the other hand, the directio-pyramidal decomposition is a versatile instrument to study motion and interaction of individual wave components in detail.

So far we have introduced the directio-pyramidal decomposition as a necessary procedure to precede the image sequence analysis for water waves. The next step will now be to apply image sequence analysis on each of the different components. It is planned to process the decomposed wave image sequences in cooperation with the German Cancer Research Center, Heidelberg (J. Dengler) and the Fraunhofer-Institut für Informations- und Datenverarbeitung, Karlsruhe (H.-H. Nagel) using algorithms developed in both institutions.

The directional decomposition is a necessary requirement for image sequence analysis of waves. It seems to be an interesting research topic, whether this preprocessing in turn leads to new and more efficient image sequence algorithms.

Presumably more and more similar complex scientific questions, which cannot be handled with conventional measuring technique, will be treated with computer vision systems as they are getting cheaper and more powerful. New applications, as the one presented here, illuminate image sequence analysis from other points of view. Hopefully, they also stimulate the classical field of image processing of natural scenes. Anyway, the analysis of images from physical objects implies a thorough consideration of the theoretical basis. This is just the trend found in image sequence analysis in general leading from phenomenology toward theoretical foundation, as recently pointed out by *Nagel* [15].

ACKNOWLEDGEMENTS

The author would like to thank all collegues who helped him to get aquainted with image sequence analysis, especially H.-H. Nagel, R. Kories, G. Zimmermann, and J. Dengler. Thanks are

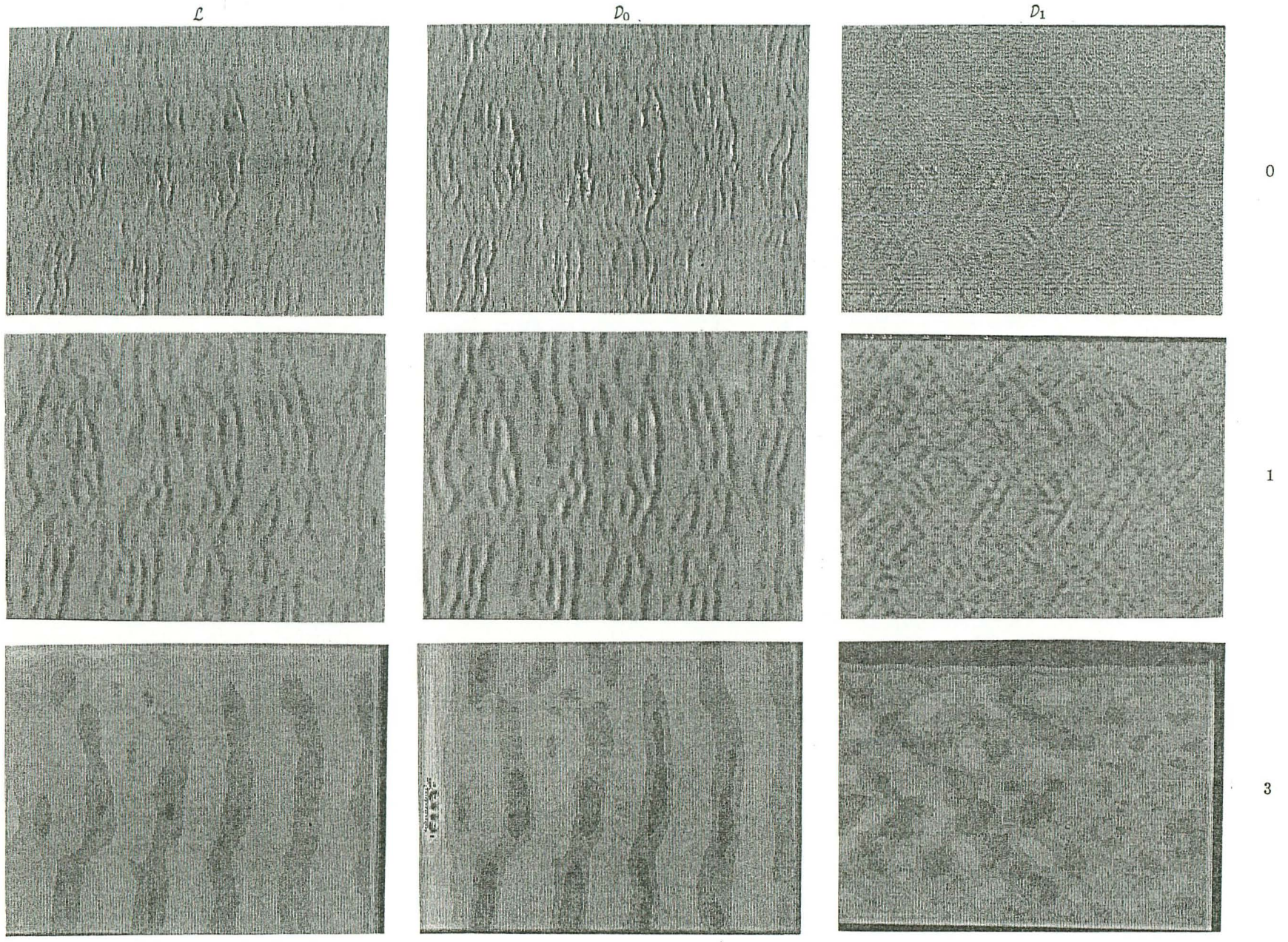

Figure 5: Directio-pyramidal decomposition of the first image in Figure 1. Levels 0, 1 and 3 of the pyramid are shown one under the other enlarged to the original size by bicubic interpolation. From left to right the isotropic Laplace level $\mathcal{L}$, and the directional components in horizontal $\mathcal{D}_0$ and vertical direction $\mathcal{D}_1$ are located.

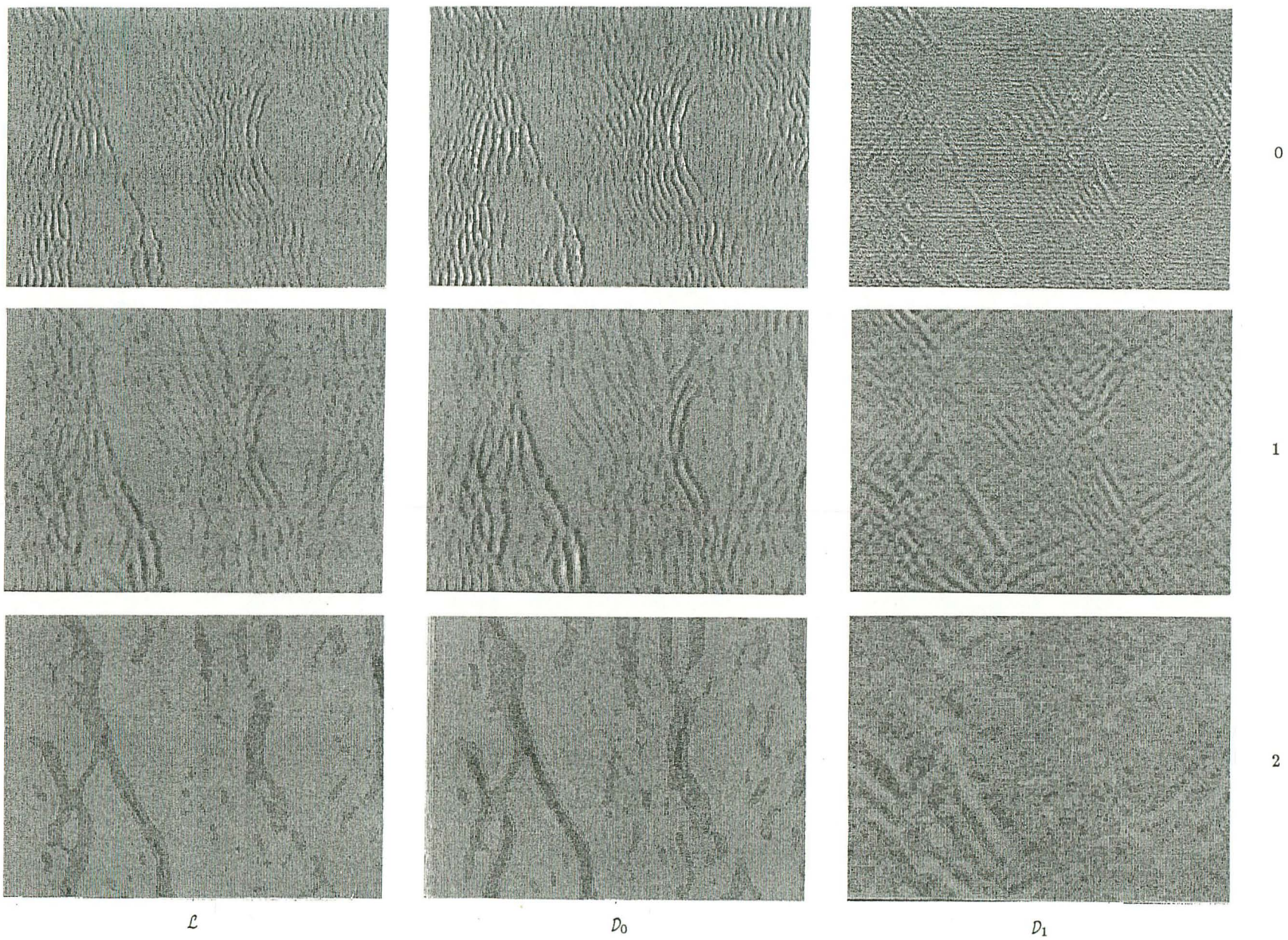

Figure 6: Same as Figure 5 for the first image in Figure 2.

also due to W. Huber who wrote the programs for the 2D-Fourier analysis and assisted the recording of the wave image sequences. The experiments were part of a cooperative project between the Centre National d'Étude Spatiale (CNES), Toulouse (A. Lifermann), the Institut de Mécanique Statistique de la Turbulence (IMST), Marseille (A. Ramamonjiarisoa), and the Institut für Umweltphysik (IUP), Heidelberg (B. Jähne). The author would like to thank the workshops of the IUP and IMST for the construction of the wave visualization system and assistance during the experiments, respectively. Financial support from the German Science Foundation and the CNES is also gratefully acknowledged.

References

[1] Banner, M. L., and O. M. Phillips, On the incipient breaking of small scale waves, *J. Fluid Mech., 65*, 647–656, 1974.

[2] Burt, P. J., The pyramid as a structure for efficient compution, in "Multiresolution Image Processing and Analysis", edited by A. Rosenfeld, Springer, New York, 1984.

[3] Dengler, J., Local motion estimation with the dynamic pyramid, 8th Intern. Conference Pattern Recognition, Paris, 1289–1292, 1986.

[4] Irani, G. B., and B. L. Gotwols, WAVDYN: Measurements of the independence of ocean wind waves, *Johns Hopkins APL Technical Digest, 3*, 49–58, 1982.

[5] Huber, W., Doctoral dissertation, Institut für Umweltphysik, University Heidelberg, in preparation, 1987.

[6] Jähne, B., Transfer processes across the free air-water interface, Habilitationsschrift, Faculty for Physics and Astronomy, University of Heidelberg, 1985.

[7] Jähne, B., Bildfolgenanalyse in der Umweltphysik: Wasseroberflächenwellen und Gasaustausch zwischen Atmosphäre und Gewässern, Proceedings of the 8th DAGM-Symposium Mustererkennung 1986, Informatik-Fachberichte 125, 201–205, 1986.

[8] Jähne, B., K. O. Münnich, R. Bösinger, A. Dutzi, W. Huber, P. Libner, On the parameters influencing air-water gas exchange, *J. Geophys. Res., 92*, 1937–1949, 1987.

[9] Keller, W. C., and B. L. Gotwols, Two-dimensional optical measurement of wave slope, *Applied Optics, 22*, 3476–3478, 1983.

[10] Kunt, M., A. Ikonomopoulus, and M. Kocher, Second-generation image-coding techniques, *Proceedings IEEE, 73*, 549–574, 1985.

[11] Knutsson, H., Filtering and reconstruction in image processing, Linköping Studies in Science and Technology. Dissertations No. 88, Linköping University, Sweden, 1982.

[12] Lifermann, A., B. Jähne, and A. Ramamonjiarisoa, Une Étude en soufflerie de la réflexion des hyperfréquences par des champs de houles et de vagues, *Oceanologica Acta*, in press, 1987.

[13] McGoldrick, L. F., Resonant interactions among capillary-gravity waves, *J. Fluid Mech., 21*, 305–331, 1965.

[14] Nagel, H.-H., Analyse und Interpretation von Bildfolgen, *Informatik-Spektrum, 8*, 178–200 and 312–317, 1985.

[15] Nagel, H.-H., Image sequences — ten (octal) years — from phenomenology towards a theoretical foundation, 8th Intern. Conference Pattern Recognition, Paris, 1174–1185, 1986.

[16] Phillips, O. M., Spectral and statistical properties of the equilibrium range in wind-generated gravity waves, *J. Fluid Mech., 156*, 505–531, 1985.

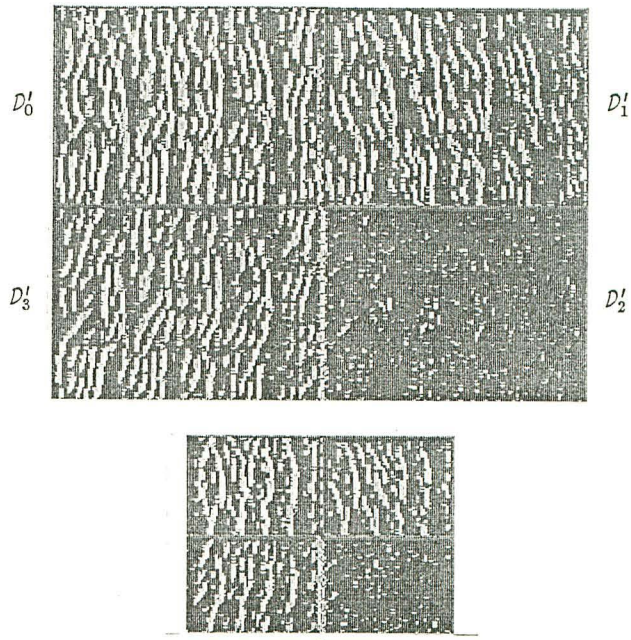

Figure 7: Directional decomposition of the first image of Figure 1 in four directional components as indicated. In two levels of the Laplace pyramid the signum of amplitude is shown.

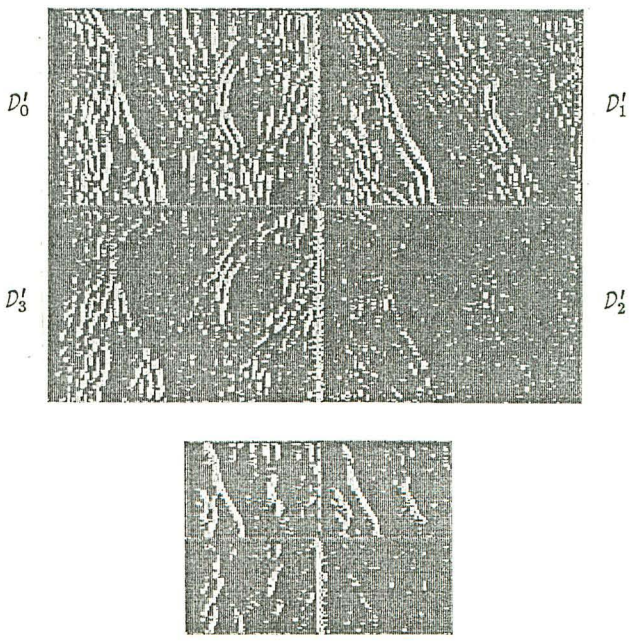

Figure 8: Same as Figure 7 for the first image in Figure 2.